

# Crystal Contact Engineering Enables Efficient Capture and Purification of an Oxidoreductase by Technical Crystallization

Phillip Grob, Max Huber, Brigitte Walla, Johannes Hermann, Robert Janowski, Dierk Niessing, Dariusch Hekmat, and Dirk Weuster-Botz\*

Technical crystallization is an attractive method to purify recombinant proteins. However, it is rarely applied due to the limited crystallizability of many proteins. To overcome this limitation, single amino acid exchanges are rationally introduced to enhance intermolecular interactions at the crystal contacts of the industrially relevant biocatalyst *Lactobacillus brevis* alcohol dehydrogenase (*LbADH*). The wildtype (WT) and the best crystallizing and enzymatically active *LbADH* mutants K32A, D54F, Q126H, and T102E are produced with *Escherichia coli* and subsequently crystallized from cell lysate in stirred mL-crystallizers. Notwithstanding the high host cell protein (HCP) concentrations in the lysate, all mutants crystallize significantly faster than the WT. Combinations of mutations result in double mutants with faster crystallization kinetics than the respective single mutants, demonstrating a synergetic effect. The almost entire depletion of the soluble *LbADH* fraction at crystallization equilibrium is observed, proving high yields. The HCP concentration is reduced to below 0.5% after crystal dissolution and recrystallization, and thus a 100-fold HCP reduction is achieved after two successive crystallization steps. The combination of fast kinetics, high yields, and high target protein purity highlights the potential of crystal contact engineering to transform technical crystallization into an efficient protein capture and purification step in biotechnological downstream processes.

## 1. Introduction

Protein crystallization concentrates the target protein to a solid, regularly structured crystal phase and impurities remain in the soluble phase. In fact, the biotechnological industry can take advantage of the process of protein crystallization to purify and formulate proteins the way it has been applied for recombinant insulin.<sup>[1,2]</sup> Due to the dense packing of proteins in the crystal, crystalline formulations exhibit longer shelf life, and require less cooling and storage volume than dissolved proteins.<sup>[3,4]</sup> Compared to preparative liquid chromatography, technical crystallization is considerably less expensive because of the relatively simple equipment that needs no expensive consumables, such as chromatographic resins.<sup>[5–14]</sup> Technical crystallization of small molecules is widely used in the chemical and biopharmaceutical industry. To date, however, the technical crystallization of proteins has been integrated in only a few biotechnological downstream processes, although it follows the same thermodynamic principles. Recently, Hubbuch et al. gave a


comprehensive picture on the latest research advances and challenges in technical or “preparative” protein crystallization for purification purposes, ranging from novel methods supporting the identification of crystallization conditions, optimization approaches for the crystallization process, and the final crystal separation process.<sup>[15]</sup> In spite of the ongoing progress in screening automation, the major bottleneck is the first step mentioned, the identification of crystallization conditions.

Previously, we demonstrated a proof of concept which addresses this hitherto empirical and elaborate screening step by rationally redesigning the protein itself instead of changing the crystallization conditions.<sup>[16]</sup> We showed that both surface entropy reduction (SER), a protein engineering strategy developed for crystallographic purpose,<sup>[17]</sup> and the introduction of charged amino acids at the crystal contact of *Lactobacillus brevis* alcohol dehydrogenase (*LbADH*) can significantly enhance crystallizability of the purified protein. The term “enhanced crystallizability” was used to compare the crystallization behavior on the  $\mu\text{L}$ -scale and represents the correlating observations of a higher number

P. Grob, M. Huber, B. Walla, J. Hermann, Dr. D. Hekmat, Prof. D. Weuster-Botz  
Technische Universität München  
Lehrstuhl für Bioverfahrenstechnik  
Boltzmannstraße 15, Garching 85748, Germany  
E-mail: dirk.weuster-botz@tum.de

Dr. R. Janowski, Prof. D. Niessing  
Helmholtz Zentrum München  
Institute of Structural Biology  
Ingolstädter Landstraße 1, Neuherberg 85764, Germany

Prof. D. Niessing  
Institute of Pharmaceutical Biotechnology  
Ulm University  
James-Franck-Ring N27, Ulm 89081, Germany

 The ORCID identification number(s) for the author(s) of this article can be found under <https://doi.org/10.1002/biot.202000010>

© 2020 The Authors. *Biotechnology Journal* published by WILEY-VCH Verlag GmbH & Co. KGaA, Weinheim. This is an open access article under the terms of the Creative Commons Attribution License, which permits use, distribution and reproduction in any medium, provided the original work is properly cited.

DOI: 10.1002/biot.202000010

of crystals (equivalent to a higher nucleation rate), lower induction time, lower time span until crystallization equilibrium, and crystallization at reduced concentrations of protein and crystallization agent. *LbADH* was chosen as an example protein because of its biocatalytic applicability in industrial enantioselective reductions of a broad range of ketones to its alcohols and its high thermal stability.<sup>[18–24]</sup>

In the present work, we aim to design further improved *LbADH* mutants that allow for a capture and purification step by protein crystallization from impure solutions, that is, from microbial cell lysate. The effect of combining single mutations in double mutants will be investigated in terms of possible synergies during technical protein crystallization.

## 2. Results

### 2.1. Selection of Single Mutants on a $\mu\text{L}$ -Scale

First, the crystallizability of the four single *LbADH* mutants K32A, Q126H, T102E, and D54F were investigated during  $\mu\text{L}$ -scale crystallization experiments. K32A and Q126H were the two best crystallizing *LbADH* mutants, which we identified in a previous study.<sup>[16]</sup> The amino acid exchange T102E was intended to generate a salt bridge (ionic interaction) between glutamic acid (E) and a facing lysine (K). Contrary to results presented in Nowotny et al.,<sup>[16]</sup> mutant T102E crystallized significantly better than the WT, applying a high variety of crystallization conditions, ranging from 0 to 5 g L<sup>-1</sup> protein and 0 to 100 g L<sup>-1</sup> polyethylene glycol monomethyl ether (PEG 550 MME). The exchange D54F was intended to generate aromatic  $\pi$ -stacking between two facing phenylalanines (F) at the crystal contact of two monomers, and thus to enhance the crystallizability.

Compared to the mutants K32A and Q126H, the mutants D54F and T102E revealed additionally enhanced crystallizability on the  $\mu\text{L}$ -scale using purified protein. The term “enhanced crystallizability” was defined as the combination of a higher number of crystals, lower induction time, lower time span until crystallization equilibrium, and crystallization at reduced concentrations of protein and crystallization agent PEG 550 MME. Preserved catalytic activity was the second selection criterion. All four single mutants exhibited enzymatic activities comparable to that of the WT, which was expected due to the large distance between the catalytic center and the four mutated positions (see Figure S1, Supporting Information). Reduced concentrations of cofactor NADPH and substrate acetophenone also resulted in catalytic activities comparable to those of WT, indicating no significant effect of the respective amino acid exchanges on the affinity of both molecules (see Figure S2, Supporting Information).

### 2.2. Stirred mL-Scale Crystallization of Single Mutants from Dialyzed Cell Lysate

*LbADH* WT and the four mutants K32A, Q126H, T102E, and D54F were produced according to the protocol for  $\mu\text{L}$ -scale crystallization of purified proteins. No deviations were observed in the *LbADH* yield *LbADH*/host cell protein (HCP) ratio, which could have biased crystallization (see Figure S3, Supporting Information). Cell disruption in phosphate-buffered saline (PBS)

and subsequent dialysis against protein buffer were conducted according to the aforementioned protocol. Affinity chromatography was the only process step that was omitted, facilitating comparability to previous crystallization results on the  $\mu\text{L}$ -scale with purified protein. The HCP concentration was approximately 50% (estimated by SDS-PAGE densitometry).

In the stirred mL-crystallizers all mutants started to crystallize earlier and reached crystallization equilibrium earlier than the WT (faster crystallization kinetics) (see Figure 1A,B). The crystallization kinetics of the mutants D54F and T102E were significantly faster than those of Q126H, K32A, and WT (T102E  $\approx$  D54F > Q126H > K32A > WT). These results match those obtained from the  $\mu\text{L}$ -scale experiments using purified protein, and thus demonstrate the scalability from the static  $\mu\text{L}$ - to the stirred mL-scale irrespective of the HCP concentration in the cell lysate. At crystallization equilibrium, almost a complete depletion of *LbADH* in the soluble phase was observed resulting in a high crystallization yield of >95% (measured by enzymatic activity assay; visualized by SDS-PAGE, see Figure 2A (Bands with a size of  $\approx$ 56 kDa in the purified samples correspond to dimerized *LbADH* monomers; reduced concentrations of reducing agent  $\beta$ -mercaptoethanol in the Laemmli SDS buffer led to a more intense “dimer” band)). No significant changes in crystallization yield were observed among the *LbADH* variants. Crystal morphologies differed significantly from each other (see Figure 1C).

Reducing the concentration of crystallizing agent PEG 550 MME and the total protein concentration by 25% each prevented WT crystallization while all single mutants still crystallized but with decreased crystallization kinetics (see Figure S4, Supporting Information).

### 2.3. Crystal Dissolution and Recrystallization of Single Mutants

Crystal slurries of the *LbADH* WT and the four single mutants were centrifuged and the crystals resuspended in protein buffer for crystal washing. Enzymatic activity assays confirmed that there was no crystal dissolution during this process. *LbADH* WT, K32A, Q126H, and T102E crystals dissolved within a few seconds, using protein buffer with a high MgCl<sub>2</sub> concentration (20 mM HEPES-NaOH pH 7.0, 1 M MgCl<sub>2</sub>). Dissolved *LbADH* crystals contained 3.0%  $\pm$  0.1% HCP (analyzed by HCP ELISA exemplary for mutant T102E), which corresponds to a more than tenfold HCP reduction compared to the initial dialyzed lysate. D54F crystals were only partially dissolvable in this buffer. After dialysis and concentration of the samples, recrystallization was conducted in the stirred mL-crystallizers. The relative crystallization kinetics of *LbADH* variants were identical to those of the stirred mL-scale experiments (compare Figures 1 and 3; T102E > [D54F] > Q126H > K32A > WT) in spite of varying starting conditions (lower *LbADH* and HCP concentrations). D54F must be regarded separately due to its significantly lower initial concentration because of its aforementioned partial crystal dissolution; however, it was shown that nucleation of this mutant occurred quickly even at an *LbADH* concentration below 1 g L<sup>-1</sup> (see Figure S5, Supporting Information).

Washed and dissolved crystals after recrystallization contained only 0.3%  $\pm$  0.0% HCP, corresponding to an additional tenfold reduction of HCP compared to the first crystallization step

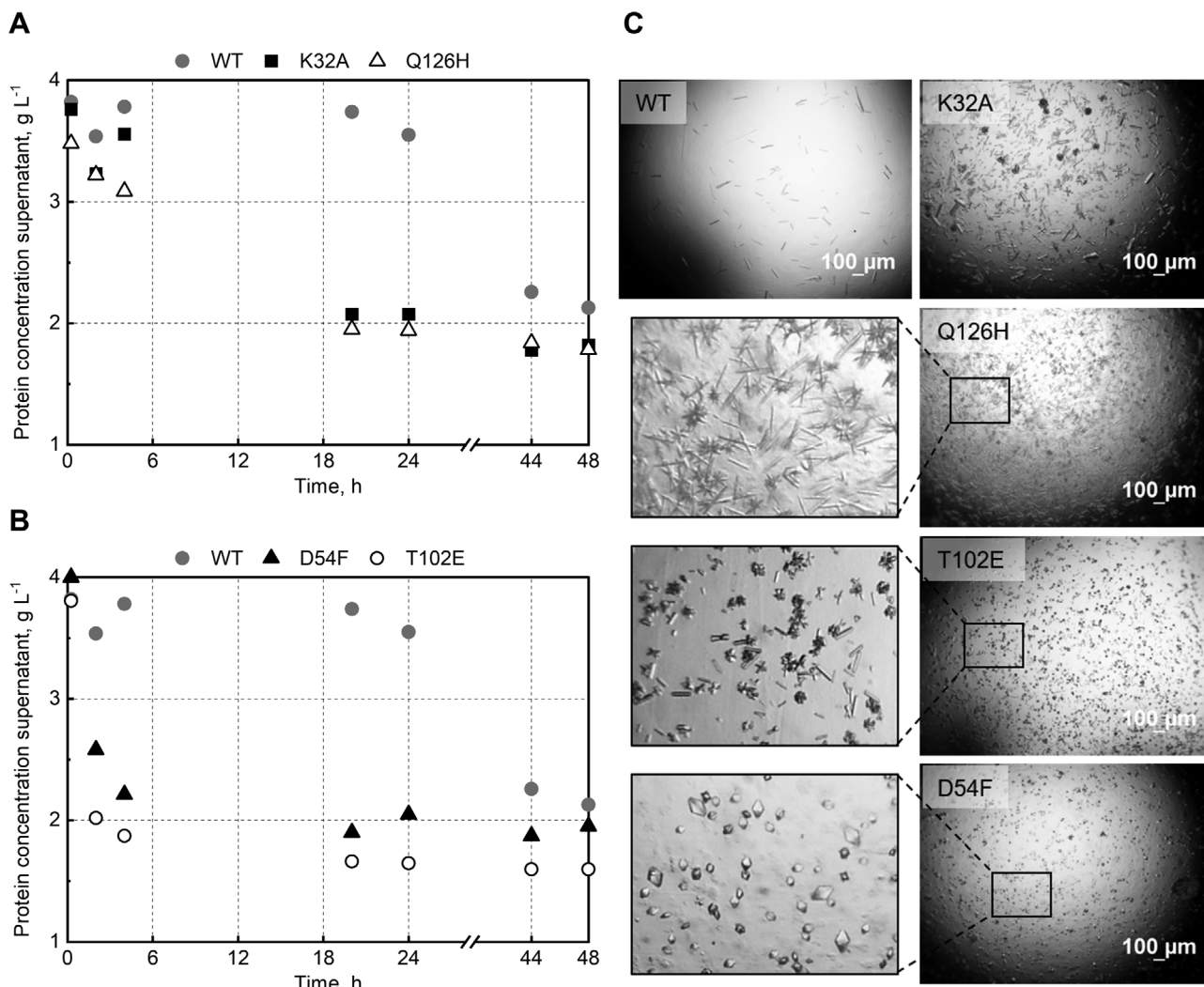


**Figure 1.** A,B) Crystallization kinetics and C) crystal microphotographs of *LbADH* WT and four single mutants from dialyzed *E. coli* cell lysate. Crystallization was conducted in five parallel stirred mL-crystallizers ( $V = 5$  mL,  $n_{\text{stirrer}} = 150$  min<sup>-1</sup>,  $100$  g L<sup>-1</sup> PEG 550 MME,  $T = 20$  °C). The protein concentration in the supernatant was measured by BCA assay. Microphotographs were taken after 24 h. The framed image sections of Q126H, T102E, and D54F are fivefold magnified.

(analyzed by HCP ELISA exemplary for mutant T102E). Recrystallization yields of >97% were observed. Crystallization and dissolution of *LbADH* variants had no measurable effect on the specific enzymatic activities (data not shown).

#### 2.4. Synergetic Effects— $\mu$ L-Scale Crystallization of Purified Double Mutants

It was investigated whether combinations of two mutations would result in double mutants with enhanced crystallizability compared to the respective single mutants. All four single *LbADH* mutants crystallized in space group *I222* or *P2<sub>1</sub>22<sub>1</sub>*, with one or two monomers in the crystallographic asymmetric unit, respectively (K32A, *I222* (PDB ID 6HLF); Q126H, *I222* (PDB ID 6Y10); T102E, *P2<sub>1</sub>22<sub>1</sub>* (PDB ID 6Y0S); and D54F, *P2<sub>1</sub>22<sub>1</sub>* (PDB

ID 6Y1C)). We previously showed that in the case of *LbADH* crystallization, both space groups result in highly similar crystal packing.<sup>[24]</sup> Five double mutants were generated: K32A\_T102E, K32A\_Q126H, D54F\_T102E, D54F\_Q126H, and T102E\_Q126H. The sixth possible combination K32A\_D54F was not considered due to the close proximity and mutual interaction of the amino acids, as it was previously shown.<sup>[16]</sup> All double mutants revealed enhanced crystallizability compared to the WT. Two double mutants (D54F\_T102E and T102E\_Q126H) exhibited enhanced crystallizability compared to both of the respective single mutants, indicating a synergetic effect in these cases (see **Figure 4**).

To validate these findings, the experimental scope was expanded by generating further double mutants. Additionally, Q126K (*I222*, PDB ID 6Y0Z; enhanced crystallizability compared to the WT<sup>[16]</sup>) and D54Y (no X-ray data available; similar crystallization behavior to D54F) were combined with

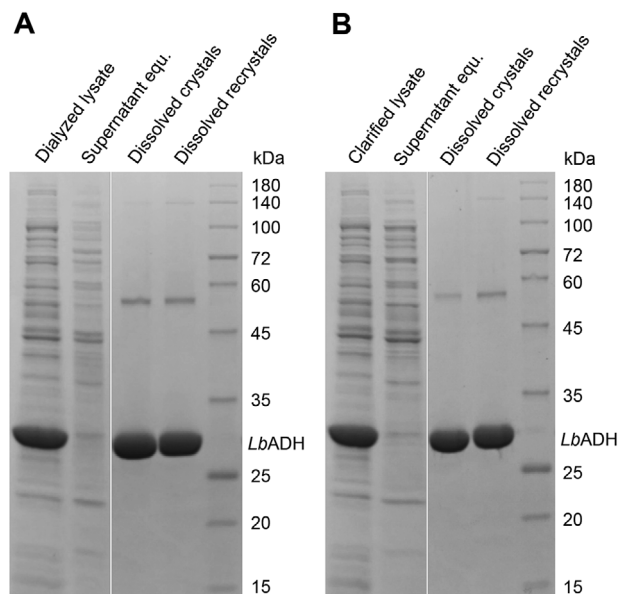


**Figure 2.** SDS-PAGE visualizing the crystallization yield and the purity effect of crystallization and recrystallization. A) Crystallization of *LbADH* T102E from dialyzed lysate. B) Crystallization of *LbADH* T102E from clarified lysate. Samples “Supernatant equ.” correspond to the supernatant in crystallization equilibrium. Bands with a size of  $\approx 56$  kDa in the purified samples correspond to dimerized *LbADH* monomers.

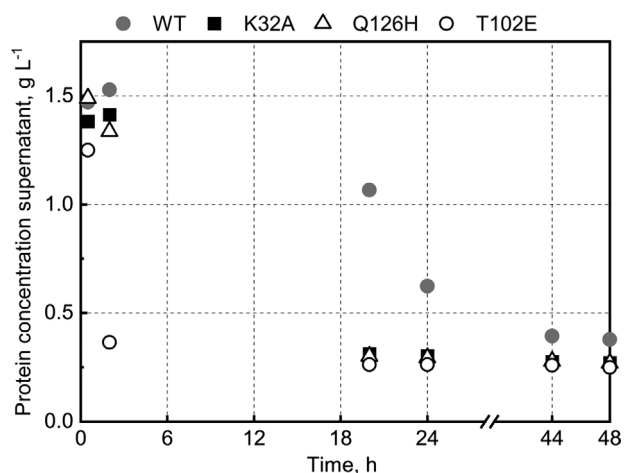


**Figure 3.** Recrystallization kinetics of *LbADH* WT and the single mutants K32A, Q126H, and T102E after crystal washing and dissolution. Crystallization was conducted in five parallel stirred mL-crystallizers ( $V = 5$  mL,  $n_{\text{stirrer}} = 150 \text{ min}^{-1}$ ,  $100 \text{ g L}^{-1}$  PEG 550 MME,  $T = 20$  °C). The protein concentration in the supernatant was measured by BCA assay. Crystal microphotographs are given in Figure S5, Supporting Information.

aforementioned single mutations to generate five additional double mutants: K32A\_Q126K, D54F\_Q126K, D54Y\_Q126H, D54Y\_Q126K, and T102E\_Q126K. These five double mutants also exhibited enhanced crystallizability compared to the WT. Three double mutants revealed enhanced crystallizability compared to that of both respective single mutants (D54Y\_Q126H, D54Y\_Q126K, and T102E\_Q126K). In summary, synergistic effects were obtained in five out of ten cases, suggesting a successful, general engineering approach. All single and double mu-

tants, which were analyzed by X-ray diffraction, crystallized in the same space group  $P2_122_1$  or  $I222$ , indicating a highly similar crystal packing (exemplarily visualized in Figure S6, Supporting Information). The data does not allow for an interpretation of why half of the double mutants did not exhibit a synergistic effect.

In comparison to that of the WT, the double mutants revealed maximum enzymatic activities between 70% and 104%, except the two double mutants with mutation D54Y (compare Figures S2 and S7, Supporting Information). Mutation D54Y significantly reduces the maximum enzymatic activities of the single mutant and both double mutants.

### 2.5. Stirred mL-Scale Crystallization of Double Mutants from Clarified Cell Lysate

The best crystallizing *LbADH* double mutants D54F\_T102E and T102E\_Q126H were directly crystallized from clarified cell lysate without performing a preceding dialysis (see Figure 5). This represents the most simplified process flow investigated in this work. *LbADH* WT and T102E were crystallized in parallel as references.

*LbADH* WT did not crystallize under this condition. T102E crystallized after a long induction phase of approximately 40 h, which was significantly longer than previously observed in the experiments using the dialyzed lysate, although concentrations of *LbADH* T102E were identical in both experiments. This observation indicates, that a dialysis step, performed in the first stirred mL-scale experiments, has a positive effect on crystallization kinetics. Most likely this is due to a decrease in small host cell components (e.g., peptides, oligonucleotides), which was not detectable by SDS-PAGE (see Figure 2). In contrast to *LbADH* WT and T102E, both double mutants crystallized immediately, which further demonstrates the scalability from the static  $\mu\text{L}$ - to the stirred mL-scale. Similarly to the crystals of the single mutants, the double mutants crystallized in distinct crystal morphologies. *LbADH* D54F\_T102E crystallized in a cubic or spherical form similar to single mutant D54F. *LbADH* T102E\_Q126H crystallized rod-like with a high aspect ratio, similar to Q126H (see Figure 5B).

Washed and dissolved crystals contained  $8.1\% \pm 0.6\%$  HCP after the first crystallization and  $0.2\% \pm 0.0\%$  after the recrystallization (exemplary for mutant T102E). Crystallization yields were comparably high to crystallization yields from dialyzed lysate ( $>95\%$ , measured by enzymatic activity assay, visualized by SDS-PAGE, see Figure 2B).

### 2.6. Mechanistic Interpretation for the Enhanced Crystallizability of *LbADH* T102E

The mutation T102E led to the fastest crystallization kinetics both in single and double *LbADH* mutants. The refined, high resolution X-ray dataset of *LbADH* T102E was compared to that of the WT to elucidate the intermolecular basis for improved crystallizability. Threonine (T102) in the WT seems not to play an important role in the crystal contact due to the distance of  $>4\text{\AA}$  from the opposite monomer. In contrast, large glutamic acid (E) in the mutant T102E is in close proximity ( $\approx 3\text{\AA}$ ) to a basic lysine (K48),

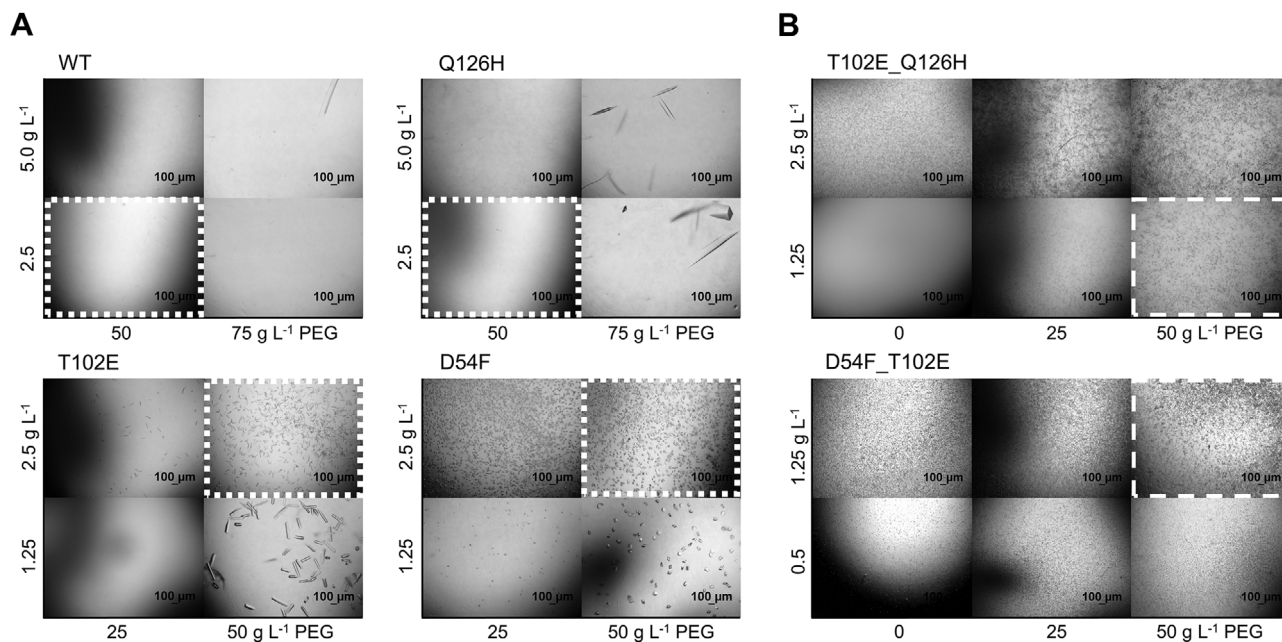


**Figure 4.** Crystallization microphotographs of purified *LbADH* WT together with the three best crystallizing single mutants A) and the two best crystallizing double mutants B) on the  $\mu\text{L}$ -scale. A) Identical crystallization conditions are illustrated by the dotted white frame. Different protein (vertical axis) and PEG 550 MME concentrations (horizontal axis) were used to illustrate the minimum concentrations where crystallization occurs. B) Identical crystallization conditions are illustrated by the dashed white frame. Both double mutants crystallized in absence of crystallization agent PEG 550 MME. Microphotographs were taken after 24 h.

presumably forming a salt bridge (see Figure 6). X-ray structural analysis of *LbADH* D54F did not confirm the assumption of an aromatic  $\pi$ -stacking between the two facing phenylalanines. Instead, both phenylalanines might interact with facing threonine (T52) (see Figure S8, Supporting Information).

### 2.7. Improved Crystallizability of *LbADH* T102E Across Different Crystallization Agents and Buffer Systems

*LbADH* WT and mutant T102E were crystallized in two commercial crystallization screens (MPD and JCSG+ suites, Qiagen, Venlo, Netherlands) to examine whether improved crystallizability of mutant T102E is restricted to the investigated standard crystallization agent PEG 550 MME. In total, 192 different crystallization buffers were tested with various pH, salts or other crystallization agents, such as 2-methyl-2,4-pentanediol (MPD) and large PEG molecules up to a molecular size of 8000 kDa. In the MPD-based screen, the amount of *LbADH* WT crystals was higher than that of mutant T102E in three cases. *LbADH* T102E crystallized with higher amount of crystals in 17 cases while *LbADH* WT did not crystallize in five cases (see Table S1, Supporting Information). A more significant result was obtained applying the JCSG+ screen. The amount of WT crystals was higher than that of mutant T102E in four cases. In contrast, T102E crystallized with higher amount of crystals in 32 cases while WT did not crystallize in 24 cases (see Table S2, Supporting Information). These findings demonstrate an improved crystallizability of *LbADH* T102E across crystallization conditions using buffers with PEG sizes from 300 to 8000 kDa, MPD as PEG substitute and pH ranges from pH 4.0–pH 8.5.

### 3. Discussion

Based on the 3D structure of *LbADH* WT, the existing crystal contacts were redesigned by targeted single amino acid exchanges to enhance intermolecular interactions. We identified the single mutants D54F and T102E, which crystallized significantly faster than the WT and faster than the previously generated mutants K32A and Q126H presented in Nowotny et al.<sup>[16]</sup> Based on X-ray structural analysis, enhanced crystallizability of the best crystallizing single mutant T102E was concluded to be the result of a newly introduced salt bridge with opposite charged lysine of the facing monomer.

All mutants crystallized significantly faster than the WT, both in purified form on the static  $\mu\text{L}$ -scale and in non-purified form from dialyzed cell lysate on the stirred mL-scale. The order of crystallization kinetics was identical (T102E  $\approx$  D54F > Q126H > K32A > WT) confirming the scalability from the static  $\mu\text{L}$ - to the stirred mL-scale irrespective of the host cell components in the cell lysate. Crystal morphologies differed significantly among *LbADH* variants, which might have a direct impact on separation processes on an industrial scale, for example, during filtration of the crystal suspension.<sup>[33]</sup> After crystallization from dialyzed cell lysate, the crystal dissolution and recrystallization were successfully conducted. Starting from an initial HCP concentration of 50%, the final HCP content was below 0.5%. High yields of >95% per crystallization step were achieved, demonstrating the implementation of an efficient chromatography-free capture and purification process for *LbADH*.

The double mutants revealed enhanced crystallizability compared to the respective single mutants in five out of ten cases. The combination of the best crystallizing single mutants

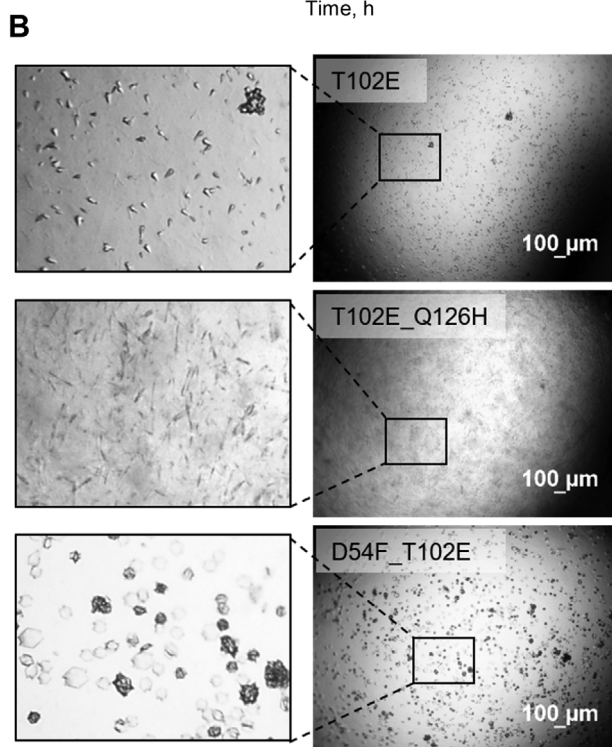
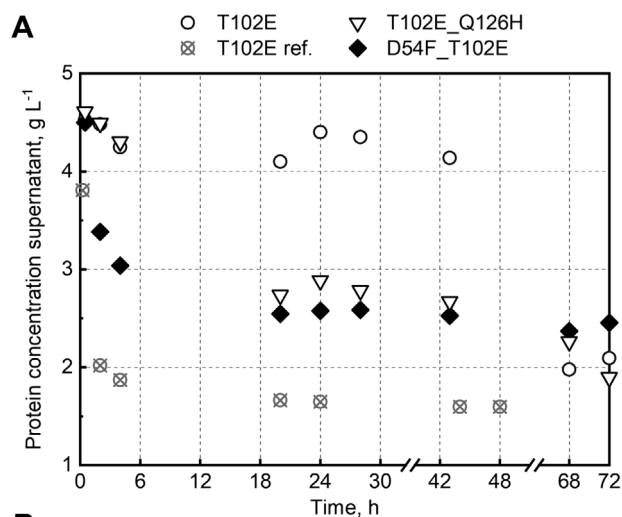


**Figure 5.** A) Crystallization kinetics from clarified cell lysate and B) crystal microphotographs of *LbADH* double mutants T102E\_Q126H and D54F\_T102E, and single mutant T102E as reference. *LbADH* WT did not crystallize under these conditions (data not shown). Crystallization was conducted in parallel stirred-tank crystallizers ( $V = 5 \text{ mL}$ ,  $n_{\text{stirrer}} = 150 \text{ min}^{-1}$ ,  $100 \text{ g L}^{-1}$  PEG 550 MME,  $T = 20^\circ\text{C}$ ). The protein concentration in the supernatant was measured by BCA assay. Microphotographs were taken after 43 h. Image sections are fivefold magnified. Dark roundish objects are agglomerates of protein crystals. Data of “T102E ref” correspond to *LbADH* T102E crystallization from dialyzed lysate (compare Figure 1).

resulted in the best crystallizing double mutants D54F\_T102E and T102E\_Q126H, demonstrating a rational, combinatorial engineering approach toward improved crystallization kinetics. The double mutants also immediately crystallized from the clarified cell lysate, which represents the harshest crystallization conditions investigated in this study; the WT did not crystallize at this

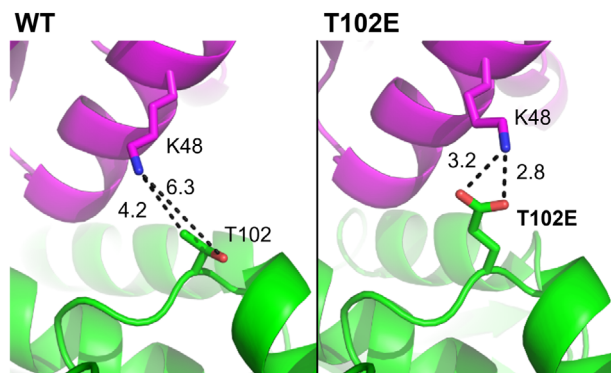


**Figure 6.** Crystallographic image illustrating the crystal contacts of *LbADH* WT and T102E. Magenta and green colored cartoon structures are sections of two *LbADH* tetramers interacting in the protein crystal. Distances (in Å) are depicted by the dashed lines. The figure was generated with the PDB IDs 6H07 (WT) and 6Y0S (T102E) using PyMOL (v.2.1; Schrödinger).

conditions and the single mutant *LbADH* T102E started to nucleate with a pronounced delay of approximately 40 h.

The results of this work emphasize the high potential of crystal contact engineering to enable and improve technical protein crystallization from highly impure cell lysate. With regard to crystallization agents, we exemplarily demonstrated for the mutant T102E that improved crystallizability is not limited to the applied crystallization agent PEG 550 MME and the applied pH of 7.0. The mutant T102E crystallizes significantly better than the WT, also by applying MPD as crystallization agent or by applying various pH levels. This could offer greater flexibility in changing process parameters in integrated crystallization processes.

Crystal contact engineering may render technical protein crystallization economically relevant for the biotechnological production of industrial proteins, because it has the potential to substitute one or more expensive preparative chromatography steps. Future work applying molecular dynamics (MD) simulations, which can predict crystallizability of in silico engineered mutants, could support the engineering approach presented here by limiting the experimental design space.

## 4. Experimental Section

**Site-Directed Mutagenesis:** The genetic basis of all mutageneses was the gene of His<sub>6</sub>-tagged wildtype (WT) *LbADH* encoded on DNA plasmid pet28a(+) as described in Hermann et al.<sup>[24]</sup> Site-directed mutagenesis was performed applying the standard QuikChange (QC)-PCR protocol with adaptations in primer design according to Zheng et al.<sup>[25]</sup> Primers used for mutant *LbADH* T102E were GAAACCGACTGCTGAATGCC (forward) and GCAGTCTCGGTTTCTTCGACAC (reverse), for D54F CACTCCTTCCAGATCAATTTTCC (forward) and GAATCTGAAAGGAGTCCGACAC (reverse), and for D54Y CACTCCTTATCAGATTCAATT TTTCC (forward) and GAATCTGATAAGGAGTGCCGACAC (reverse). Primers for *LbADH* K32A, Q126H, and Q126K were previously published in Nowotny et al.<sup>[16]</sup> All double mutations were introduced by two respective consecutive QC-PCR runs. After DpnI digestion, *E. coli* DH5 $\alpha$  transformation, and plasmid DNA extraction, plasmid DNA sequencing verified correct DNA mutations.

**Production and Further Processing of *LbADH* Variants:** Recombinant production with *E. coli* BL21 (DE3) of all *LbADH* variants, dialysis, and purification via immobilized metal affinity chromatography for experiments

on the  $\mu\text{L}$ -scale were conducted as described in Nowotny et al.<sup>[16]</sup> For the first part of the stirred mL-scale experiments using dialyzed cell lysate, cell disruption was performed in 10 mL PBS, pH 7.4 ( $25\text{--}30\text{ g L}^{-1}$  cell dry weight) by sonication ( $3 \times 3\text{ min}$ , 90% intensity, 50% pulse, Sonoplus HD 2070 and Micro tip MS 72, BANDELIN electronic, GmbH & Co. KG, Berlin, Germany) prior to dialysis against protein buffer (20 mM HEPES-NaOH pH 7.0, 1 mM  $\text{MgCl}_2$ ). For the second part of the stirred mL-scale experiments using clarified cell lysate, cell disruption was directly conducted in 10 mL protein buffer under identical conditions. Before crystallization, all samples were centrifuged for 60 min at 12 000 g and 20 °C.

**Crystallization of LbADH Variants:** The batch crystallization of purified LbADH variants on the  $\mu\text{L}$ -scale was conducted as described in Nowotny et al.<sup>[16]</sup> but with an increased number of crystallization conditions. The crystallization buffer was composed of 100 mM Tris-HCl at pH 7.0, 50 mM  $\text{MgCl}_2$ , and varying concentrations of PEG 550 MME between 0 and 200  $\text{g L}^{-1}$ . The LbADH concentrations in the protein buffer were measured spectrophotometrically at 280 nm using a calculated extinction coefficient of  $19\,940\text{ M}^{-1}\text{ cm}^{-1}$  and adjusted by ultrafiltration between 1 and 10  $\text{g L}^{-1}$ . Crystallization experiments were started by adding 5  $\mu\text{L}$  of crystallization buffer to the same volume of protein solution in 96-well  $\mu\text{L}$  batch crystallization plates (MRC UnderOil Crystallization Plate, SWISSCI, Neuheim, Switzerland). Plates were sealed with transparent adhesive tape and mounted on a light microscope, which was placed in a 20 °C incubator.

Non-purified LbADH variants in the dialyzed or clarified cell lysate were crystallized in parallel stirred 5-mL-crystallizers with a stirrer speed of 150 rpm as described in Smejkal et al.<sup>[7]</sup> Up to 5 crystallizers were operated in parallel. The photometric absorption at 280 nm of all samples was adjusted by dilution of samples with protein buffer. SDS-PAGE of cell lysates was used to verify identical LbADH concentrations and HCP/LbADH ratios. Total crystallization volume was 5 mL comprising 2.5 mL of the clarified lysate and 2.5 mL of the crystallization buffer (100 mM Tris-HCl at pH 7.0, 50 mM  $\text{MgCl}_2$ , 150 or 200  $\text{g L}^{-1}$  PEG 550 MME). The stirred mL-crystallizers were placed in a temperature-controlled water bath at 20 °C.

For LbADH WT and mutant T102E, an empiric crystallization screening was conducted at 20 °C applying the sitting-drop vapor diffusion method and two commercial screens (MPD (Cat No./ID: 130706) and JCSG+ Suite (Cat No./ID: 130720), Qiagen, Venlo, Netherlands), each with 96 different conditions (see Tables S1 and S2, Supporting Information). 0.2  $\mu\text{L}$  of purified LbADH solution ( $3.5\text{ g L}^{-1}$ ) was added to 0.2  $\mu\text{L}$  of the respective crystallization buffer. The reservoir contained 80  $\mu\text{L}$  of the crystallization buffer. Pipetting was conducted by a mosquito nanodrop dispenser (SPT Labtech, Melbourn, England). The crystallization screening was performed at the X-ray crystallography platform at Helmholtz Zentrum München.

**Crystal Dissolution and Recrystallization:** After reaching crystallization equilibrium, the crystal suspensions of the stirred mL-scale experiments were centrifuged (16000 g, 20 °C, 3 min) and the supernatant was discarded. Protein buffer was added, the crystal pellet was resuspended, centrifuged again, and the supernatant discarded. 20 mM HEPES and 1 M  $\text{MgCl}_2$  were added with the fourfold of the initial crystal suspension volume to dissolve the protein crystals. The samples were dialyzed against protein buffer and concentrated via ultrafiltration to obtain a volume of 2.5 mL. The spectrophotometric absorption at 280 nm of all samples was adjusted and recrystallization was started in stirred 5-mL-crystallizers by adding 2.5 mL of crystallization buffer (100 mM Tris-HCl pH 7.0, 50 mM  $\text{MgCl}_2$ , 200  $\text{g L}^{-1}$  PEG 550 MME) to 2.5 mL of LbADH solution.

**Protein and Crystal Analysis:** The preserved catalytic activity of LbADH variants was validated by an enzymatic activity assay in 96-well microtiter plates. The catalyzed oxidation of the cofactor NADPH was recorded spectrophotometrically (extinction coefficient NADPH at 340 nm:  $6.22\text{ mL } \mu\text{mol}^{-1}\text{ cm}^{-1}$ ), during reduction of the substrate acetophenone to 1-phenylethanol at 25 °C (Multiskan FC Microplate Photometer, Thermo Fisher Scientific, Darmstadt, Germany). 20  $\mu\text{L}$  of LbADH solution ( $6 \times 10^{-3}\text{ g L}^{-1}$  LbADH in the protein buffer) were added to 180  $\mu\text{L}$  of protein buffer containing 2.5 or 10 mM acetophenone and 0.1 or 0.5 mM NADPH. These assay conditions enabled fast and reproducible measurements and there was no need for rebuffing (the selected conditions did not aim for the highest achievable enzymatic activities).  $V_{\text{max}}$  of LbADH WT is

$24.9 \pm 3.0\text{ U mg}^{-1}$  with 10 mM acetophenone and 0.5 mM NADPH at 25 °C and pH = 7.0 ( $n = 6$  biological replicates; triplicate measurements).

Crystallization on the  $\mu\text{L}$ -scale was validated by automated microscopic imaging as described previously.<sup>[16]</sup> Stirred crystallization on the mL-scale was analyzed by microscopy (detection of the presence of protein crystals; crystal morphology), bicinchoninic acid (BCA) protein assay (remaining total protein concentration in the supernatant), enzymatic activity assay (crystallization yield in equilibrium), HCP ELISA (HCP concentration in the dissolved crystals after crystallization and recrystallization) (*E. coli* BL21 (DE3) 360-HCP ELISA type D, BioGenes GmbH, Berlin, Germany), and SDS-PAGE (verification of LbADH purity and yield). Samples were taken regularly, diluted by 1:10 to prevent further nucleation and crystal growth, and centrifuged for 3 min at 16000 g and 20 °C prior to protein concentration analysis of the supernatant.

**X-Ray Diffraction Data Collection, Processing, and Refinement:** All crystals used for structural X-ray analysis were obtained from the crystallization experiments with purified LbADH. After selecting the largest singular crystals, X-ray diffraction experiments were performed. The crystals were mounted on a nylon fiber loop and flash-cooled to 100 K in liquid nitrogen. The cryoprotection was performed for two seconds in the crystallization buffer supplemented with 25–30% (v/v) ethylene glycol. Diffraction data was collected on the PXIII X06DA beamline (PSI, Villigen, Switzerland). All measurements were performed at 100 K. X-ray diffraction data sets were collected to 1.4 Å resolution for T102E, 1.4 Å for K32A\_Q126K, and 1.8 Å for T102E\_Q126K. All data sets were indexed, integrated and scaled using XDS<sup>[26]</sup> and AIMLESS.<sup>[27]</sup> The structures were solved and refined using the CCP4 software suite (version 7.0).<sup>[28]</sup> An in silico mutated structure of PDBID 6HO7<sup>[24]</sup> served as search model for molecular replacement with Phaser.<sup>[29]</sup> Model rebuilding was performed in COOT.<sup>[30]</sup> Further refinement was done with REFMAC.<sup>[31]</sup> The final structure was validated with PDB-REDO.<sup>[32]</sup> Atomic coordinates and structure factors were deposited in the Protein Data Bank under accession codes 6Y0S (T102E), 6Y1B (K32A\_Q126K), and 6Y15 (T102E\_Q126K) (see Table S3, Supporting Information).

## Supporting Information

Supporting Information is available from the Wiley Online Library or from the author.

## Acknowledgements

The authors thank the German Research Foundation (DFG) for funding of research project WE2715/14-1 within the framework of priority program SPP 1934. Support of P.G. and J.H. by the TUM Graduate School is gratefully acknowledged. Assistance of Daniel Bischoff in X-ray data refinement is highly appreciated.

## Conflict of Interest

The authors declare no conflict of interest.

## Keywords

crystal contact engineering, downstream processing, protein purification, technical crystallization

Received: February 24, 2020

Revised: March 19, 2020

Published online:

- [1] J. Brange, *Galenics of Insulin: The Physico-chemical and Pharmaceutical Aspects of Insulin and Insulin Preparations*, Springer, Berlin, Germany **1987**.
- [2] R. G. Harrison, P. Todd, S. R. Rudge, D. P. Petrides, *Bioseparations Science and Engineering*, 2nd ed., Oxford University Press, Oxford **2015**.
- [3] B. Shenoy, Y. Wang, W. Shan, A. L. Margolin, *Biotechnol. Bioeng.* **2001**, 73, 358.
- [4] S. K. Basu, C. P. Govardhan, C. W. Jung, A. L. Margolin, *Expert Opin. Biol. Ther.* **2004**, 4, 301.
- [5] D. Hebel, S. Huber, B. Stanislawski, D. Hekmat, *J. Biotechnol.* **2013**, 166, 206.
- [6] D. Hebel, M. Ürdingen, D. Hekmat, D. Weuster-Botz, *Cryst. Growth Des.* **2013**, 13, 2499.
- [7] B. Smejkal, B. Helk, J.-M. Rondeau, S. Anton, A. Wilke, P. Scheyerer, J. Fries, D. Hekmat, D. Weuster-Botz, *Biotechnol. Bioeng.* **2013**, 110, 1956.
- [8] B. Smejkal, N. J. Agrawal, B. Helk, H. Schulz, M. Giffard, M. Mechelke, F. Ortner, P. Heckmeier, B. L. Trout, D. Hekmat, *Biotechnol. Bioeng.* **2013**, 110, 2452.
- [9] D. Hekmat, *Bioprocess Biosyst. Eng.* **2015**, 38, 1209.
- [10] P. Neugebauer, J. G. Khinast, *Cryst. Growth Des.* **2015**, 15, 1089.
- [11] M. Groß, M. Kind, *Chem. Eng. Technol.* **2016**, 39, 1483.
- [12] D. Hekmat, M. Huber, C. Lohse, N. von den Eichen, D. Weuster-Botz, *Cryst. Growth Des.* **2017**, 17, 4162.
- [13] M. B. Groß, M. Kind, *Cryst. Growth Des.* **2017**, 17, 3491.
- [14] M. B. Groß, M. Kind, *J. Cryst. Growth* **2018**, 498, 160.
- [15] J. Hubbuch, M. Kind, H. Nirschl, *Chem. Eng. Technol.* **2019**, 42, 2275.
- [16] P. Nowotny, J. Hermann, J. Li, A. Krautenbacher, K. Klöpfer, D. Hekmat, D. Weuster-Botz, *Cryst. Growth Des.* **2019**, 19, 2380.
- [17] Z. S. Derewenda, P. G. Vekilov, *Acta Crystallogr. Sect. D Biol. Crystallogr.* **2006**, 62, 116.
- [18] W. Hummel, in *New Enzymes for Organic Synthesis* (Ed: S. Thomas), Springer, Berlin, Germany **1997**, pp. 145–184.
- [19] K. Niefind, J. Müller, B. Riebel, W. Hummel, D. Schomburg, *J. Mol. Biol.* **2003**, 327, 317.
- [20] N. H. Schlieben, K. Niefind, J. Müller, B. Riebel, W. Hummel, D. Schomburg, *J. Mol. Biol.* **2005**, 349, 801.
- [21] S. Bräutigam, D. Dennewald, M. Schürmann, J. Lutje-Spelberg, W.-R. Pitner, D. Weuster-Botz, *Enzyme Microb. Technol.* **2009**, 45, 310.
- [22] D. Dennewald, W.-R. Pitner, D. Weuster-Botz, *Process Biochem.* **2011**, 46, 1132.
- [23] C. Rodríguez, W. Borzęcka, J. H. Sattler, W. Kroutil, I. Lavandera, V. Gotor, *Org. Biomol. Chem.* **2014**, 12, 673.
- [24] J. Hermann, P. Nowotny, T. E. Schrader, P. Biggel, D. Hekmat, D. Weuster-Botz, *Acta Crystallogr. Sect. F Struct. Biol. Commun.* **2018**, 74, 754.
- [25] L. Zheng, U. Baumann, J.-L. Reymond, *Nucleic Acids Res.* **2004**, 32, e115.
- [26] W. Kabsch, *Acta Crystallogr. Sect. D Biol. Crystallogr.* **2010**, 66, 133.
- [27] P. R. Evans, G. N. Murshudov, *Acta Crystallogr. Sect. D Biol. Crystallogr.* **2013**, 69, 1204.
- [28] M. D. Winn, C. C. Ballard, K. D. Cowtan, E. J. Dodson, P. Emsley, P. R. Evans, R. M. Keegan, E. B. Krissinel, A. G. W. Leslie, A. McCoy, S. J. McNicholas, G. N. Murshudov, N. S. Pannu, E. A. Potterton, H. R. Powell, R. J. Read, A. Vagin, K. S. Wilson, *Acta Crystallogr. Sect. D Biol. Crystallogr.* **2011**, 67, 235.
- [29] A. J. McCoy, R. W. Grosse-Kunstleve, P. D. Adams, M. D. Winn, L. C. Storoni, R. J. Read, *J. Appl. Crystallogr.* **2007**, 40, 658.
- [30] P. Emsley, B. Lohkamp, W. G. Scott, K. Cowtan, *Acta Crystallogr. Sect. D Biol. Crystallogr.* **2010**, 66, 486.
- [31] G. N. Murshudov, P. Skubák, A. A. Lebedev, N. S. Pannu, R. A. Steiner, R. A. Nicholls, M. D. Winn, F. Long, A. A. Vagin, *Acta Crystallogr. Sect. D Biol. Crystallogr.* **2011**, 67, 355.
- [32] R. P. Joosten, F. Long, G. N. Murshudov, A. Perrakis, *IUCrj* **2014**, 1, 213.
- [33] B. Radel, M. Funck, T. H. Nguyen, H. Nirschl, *Chem. Eng. Sci.* **2019**, 196, 72.